Drag constants for common indoor bioaerosols

L.T. Wong, H.C. Yu, K.W. Mui, W.Y. Chan

Department of Building Services Engineering, The Hong Kong Polytechnic University,

Hong Kong, China

*Corresponding author:

K. W. Mui, Department of Building Services Engineering, The Hong Kong Polytechnic University, Hong Kong, China

E-mail: behorace@polyu.edu.hk; Tel: (852) 2766 7783; Fax: (852) 2765 7198

Running heads:

Drag Constants for Common Indoor Bioaerosols

Abstract

In practice, particle drag coefficient is usually calculated using empirical relations generalizing experimental data. This study demonstrates that using the FLUENT default Stokes' law settings to computationally predict drag coefficients for bioaerosol deposition is not promising: the average fractional bias is 7% and the average normalized mean square error is 15%. Comparatively, errors for bacteria (−12% to 24%) are larger than those for fungi (–8% to 26%). These errors, however, can be minimized by a suitable choice of drag constant which can be determined by use of the bioaerosol diameter. It is shown that bacteria are associated with average drag constants (0.25 to 3.1) much lower than 24, whereas fungi generally have larger drag constants in a wider range. This study also investigates the correlation between drag coefficient and particle Reynolds number for common indoor bioaerosols with diameters in between 0.69 μm and 8.6 μm. The outcome serves as a good reference point for estimating the deposition distribution patterns of various common indoor bioaerosols.

Keywords

drag coefficient, bioaerosol deposition, bioaerosol drag constant

Nomenclature:

CFD	computational fluid dynamics
CFU	colony forming unit
MEA	malt extract agar
PCA	principal component analysis
RA	relative abundance
RNG	renormalization group
SEM	scanning electron microscope images
TSA	tryptone soya agar
TSB	tryptone soya broth
A_b	bioaerosol projected area
C_D	drag coefficient
C_s	simulated fractional bioaerosol count
C_e	measured fractional bioaerosol count
d_b	bioaerosol diameter
$F_D(u-u_b)$	drag force per unit particle mass
F_x	additional acceleration
g	gravity force
h^{-1}	per hour
ij	array coordinates
K	bioaerosol drag constant
l	chamber length
l_1	length of bioaerosols
l_2	width of bioaerosols
l_b	aspect ratio of bioaerosols
ms^{-1}	meter per second
p	p-value
R	correlation coefficient
Re	Reynolds number
T	absolute temperature of the fluid
t	t-test value
u_b	bioaerosol velocity
u	fluid parcel velocity
w	chamber width
x/l	chamber fractional length
y/w	chamber fractional width
ρ_b	bioaerosol density
ρ	carrier phase density
μ	molecular viscosity of the carrier phase

$\phi_{e,ij}$	total counts of bioaerosols at location ij
$\phi_{s,i}$	simulated bioaerosol deposition distribution
$\phi_{e,i}$	measured bioaerosol deposition distribution
ε_1	fractional bias
ε_2	normalized mean square error

1. Introduction

Bioaerosols may consist of pathogenic and non-pathogenic live or dead bacteria, fungi, viruses, protozoa, pollen, etc. Exposures to bioaerosols are associated with a wide range of adverse health effects including infectious diseases, acute toxic effects, allergies and cancer. Apart from the dispersion of bioaerosols, understanding the deposition of bioaerosols in ventilated environments can significantly improve our current knowledge of pathogen transport [1] Although computational fluid dynamics (CFD) has become a powerful tool for studying particle deposition [2-5], conclusive information about the aerodynamic properties of common indoor bioaerosols is still lacking. Indeed, there are health and safety concerns as well as practical difficulties in directly obtaining information on the aerodynamic properties and the drag coefficients for bioaerosol particles using Class I and Class II biological experimental facilities[6, 7].

Physical forces acting on a bioaerosol particle in motion are atmospheric drag which usually tends to slow the particle from the bulk air velocity and changes with gravity as well as the particle size and shape. Existing methods available to determine particle size and shape range from very simple but commonly used approaches (e.g. determination of shape factors such as aspect and elongation ratios) to very sophisticated measures (e.g. Principal Component Analysis (PCA), Clustering, and Fourier Analysis) [8]. Reportedly, different image analysis programs have marked influences on the shape factor values obtained [9]. Igathinathane et al. developed an

ImageJ plugin that extracts the dimensions from a digital image of disjoint particles after identifying their shapes and determines their particle size distribution [10]. Blott and Pye also re-examined the basic concepts of particle shape and suggested a number of new and modified methods which are widely applicable to a range of sedimentological problems [11].

In a previous study, an Eulerian-Lagrangian approach was used for predicting the deposition of bioaerosols in a ventilated chamber and the experimental results agreed well with the modeling ones in spite of some disparities [12]. Based on that approach, this study developed mathematical expressions to define drag coefficients of common indoor bioaerosols for CFD studies. Furthermore, the correlation between drag coefficient and Reynolds number for common indoor bioaerosols with diameters in between 0.69 μm and 8.6 μm was investigated.

2. Drag coefficient and numerical study

Drag coefficient correlations in uniform flow around a sphere are a staple of fluid flow calculations and fluid mechanics education. Drag coefficients C_D are applied in numerical models to calculate pressure drops and flow rates for settling flows around spheres. However, the correlation between the drag coefficient and Reynolds number of common indoor bioaerosols has not yet been fully understood. Theoretically, the motion of bioaerosols can be calculated by integrating the force balance on the bioaerosols in

terms of drag F_D, gravity g and additional acceleration F_x (if any) as given below, where u_b and u are the velocities of the bioaerosols and a fluid parcel respectively, ρ_b is the bioaerosol density, ρ is the carrier phase density, μ is the molecular viscosity of the carrier phase, d_b is the bioaerosol diameter and Re is the Reynolds number for bioaerosols,

$$\frac{du_b}{dt} = F_D(u - u_b) + \frac{g(\rho_b - \rho)}{\rho_b} + F_x;\ F_D = \frac{18\mu}{d_b^2 \rho_b} \times \frac{C_D Re}{24};\ Re = \frac{\rho d_b |u_b - u|}{\mu} \quad \ldots (1)$$

When a particle is in motion in the atmosphere, it is subject to inertia (Newton's law of resistance) and drag effects. For small sized particles, viscous forces dominate and Stokes' law can be adopted (Re<1). Using Stokes' law and a constant K=24 for particle simulations, the drag coefficient is a function of Reynolds number Re,

$$C_D = \frac{K}{Re};\ Re < 0.1 \quad \ldots (2)$$

The bioaerosol drag constant K, a bioaerosol particle constant suitable for CFD based on particle simulations, can be determined by minimizing the discrepancy between simulated and measured fractional bioaerosol counts C_s and C_e in the controlled experiments, i.e. by setting the error term $\varepsilon_1 = 0$ or the derivative of the error

term ε_2 $\frac{\partial \varepsilon_2}{\partial K} = 0$. This constant *K* reflects the drag of bioaerosol particles – single-celled organisms such as bacteria – in numerical computations using equivalent particle diameter. The goodness of fit of the chosen constant can be examined from the fractional bias ε_1 – a measure of the over- or under-prediction of a model, and the normalized mean square error ε_2 – a measure of the relative fit of a model to the measured data, where *N* is the number of simulation-measurement data pairs [13],

$$\varepsilon_1 = \frac{1}{N} \sum \frac{C_e - C_s}{\frac{1}{2}\left(C_e + C_s\right)} \quad \ldots (3)$$

$$\varepsilon_2 = \frac{1}{N} \sum \frac{\left(C_e - C_s\right)^2}{C_e C_s} \quad \ldots (4)$$

2.1 Numerical simulations

In this study, numerical simulations were performed in a small chamber of size 0.650 m (L) × 0.380 m (W) × 0.284 m (H) using a commercial finite volume based CFD code FLUENT (version 6.3–2006) based on an Eulerian-Lagrangian approach as adopted in a previous study [12]. The simulated longitudinal bioaerosol deposition distributions on the chamber floor $\phi_{s,i}$ at a horizontal distance i=1,…,7 from the inlet e_1 were recorded in a setup as shown in Figure 1. In brief, the convection term was discretized using a second order upwind scheme. The PISO algorithm was adopted to

couple the pressure and velocity fields. Renormalization group (RNG) *k*-ε model was selected to model turbulent flow. A grid system with mesh size 320 k (grid convergence index 4.9%) was used [14]. As the deposition process was very slow, airflow and particle motions were modeled under steady-state conditions. To model the discrete phase transport, a Lagrangian scheme was employed. In the simulations, tracer bioaerosols were injected continuously through a high sidewall inlet and exhausted through an outlet aligned on the opposite wall.

Studies of fine particles (e.g. <1 μm) have shown that coagulation will be significant only at high particle concentrations (e.g. >20,000 cm^{-3}) and can be ignored at low particle concentrations (≤3,000 cm^{-3}) [15, 16]. As the bioaerosol concentrations in the chamber were kept at a very low volume fraction (<1 CFU cm^{-3}), the coagulation effect of bioaerosol particles on turbulent flow was assumed neglectable in this study. Bioaerosol samples collected in the experiments were examined under a compound light microscope to verify the assumption.

Each bioaerosol released from the injection site was tracked separately for its position, velocity and residence time. Deposition was assumed for all particles touching a surface and no resuspension was considered. Simulations were repeated 10 times to determine the average deposition distribution pattern. It was noted that for bioaerosol densities ranging from 1.1 to 1.3 g cm^{-3}, there was insignificant influence on the deposition patterns on the small chamber floor [12, 17]. Bioaerosol density ρ_b is

therefore assumed to be 1.1 g cm^{-3}. This model assumes successive encounter of particles with discrete turbulence eddies and the eddy interaction time scale can be found elsewhere.

3. Experiments with common indoor bioaerosols

Bioaerosol deposition distribution patterns on the chamber floor $\phi_{e,i}$ were also measured experimentally in a 70L tempered glass ventilated chamber of size 0.650 m (L) × 0.380 m (W) × 0.284 m (H). The chamber was sealed and placed inside a Class II biological safety cabinet as shown in Figure 1. The leakage rate tested under atmospheric pressure was 2.4×10^{-3} min^{-1}. Agar plates (i.e. TSA for bacteria and MEA for fungi) organized in an array of 7 columns by 4 rows were laid on the chamber floor to record the deposition patterns [17].

Airborne bacterial and fungal genera in Table 1 were found common in air-conditioned buildings with relative abundances (RA) of up to 100% in air samples. The bacterial species investigated were *Aeromonas hydrophila*, *Bacillus atrophaeus* (ATCC 9372), *Campylobacter jejuni*, *Escherichia coli* (ATCC 10536), *Micrococcus luteus* (ATCC 4698), *Salmonella typhimurium* (ATCC 14028), *Serratia marcescens* (ATCC 6911) and *Staphylococcus aureus* (ATCC 6538), while the fungal species examined were *Alternaria alternata* (ATCC 6663), *Aspergillus niger*, *Cladosporium cladosporioides* (ATCC 16021), *Penicillium citrinum* (ATCC 6849) and *Rhizopus* sp.

[18-28]. Among the tested bioaerosols, *Aspergillus*, *Cladosporium*, *Micrococcus*, *Penicillium* and *Staphylococcus* were more abundant than the rest. All of the bioaerosols were globose, ovoid or elliptical; their scanning electron microscope (SEM) images are illustrated in Figure 2. As there are practical difficulties in the computation of particle deposition using the concept of an aerodynamic diameter for non-spherical bioaerosols, a concept of equivalent particle diameter was applied in this study, i.e. the projected image area A_b , length l_1 and width l_2 of the bioaerosols were determined from a number of SEM images using a method (ImageJ) developed by the National Institutes of Health (NIH). The equivalent bioaerosol diameter d_b (with standard error) and aspect ratio l_b as presented in Table 1 are given by [29, 30],

$$d_b = 2\sqrt{\frac{A_b}{\pi}};\ l_b = \frac{max(l_1, l_2)}{min(l_1, l_2)} \quad \ldots (5)$$

A specific method was employed for the preparation of vegetative bacterial cells [28]. Initially, the bacterial cultures were inoculated onto Tryptone Soya Agar (TSA) and incubated at 30°C for 24 hours. A single colony was then picked from the TSA, inoculated into 10 ml Tryptone Soya Broth (TSB) and incubated at 30°C under aerobic conditions for another 24 hours. Similarly, the fungal cultures were inoculated onto 2% Malt Extract Agar (MEA) and incubated at 25°C for 1 week. After that, a single colony

was picked and inoculated onto another 2% MEA plate which in turn was incubated at 25°C for a further week.

For the bioaerosol particles less than 3 μm, a 50 ml bacterial/fungal suspension was stored in a collision nebulizer for aerosolization. By spreading its serially diluted samples (made in sterile Ringer's solution) onto agar plates for counting after incubation, the suspension was tested for sufficient amount of viable cells. In this study, the average concentrations of the bacterial and fungal suspensions were 6×10^5 CFU ml^{-1} and 2×10^4 CFU ml^{-1} respectively. For the bioaerosol particles larger than 3 μm, an aerosolization box of size 0.145 m (L) × 0.145 m (W) × 0.065 m (H) with a mixing fan inside (Figure 1) was used to generate bioaerosols (Lai et al. 2012). An air jet was directed to the cultured fungi (from diluted suspension of 240 spores on 20-mm thick MEA) placed on the floor of the aerosolization box. To prepare the fungal bioaerosols, a fungal spore was incubated in a container for a week and its cultures were observed every day under a compound light microscope. A culture was suitable for aerosolization when the spores were mature (brownish black) and the sporangium wall was broken. Preliminary tests were carried out to investigate the suitable time for aerosolizing the cultures without mycelium formation. A glass slide with gelatin gel was placed inside the chamber directly facing the inlet to collect the spores generated. The slide was then stained with lactophenol cotton blue and examined under a compound light microscope (400X).

During the experiment, compressed air, first filtered through an air filtration system “a” (Model 3074B, TSI) for moisture and impurities removal, entered the cabinet via two airflow paths f_1 (variable flow rates) and f_2 (a constant flow rate of 2 L min^{-1}) and then passed into airflow path f_3. f_1 was for the adjustment of aerosol concentration by volume, while f_2 was connected to a 6-jet collision nebulizer “c” for bioaerosol particles less than 3 μm or to the aerosolization box described above for bioaerosol particles larger than 3 μm. The set up produced dry monodispersed bioaerosols to minimize coagulation. The volume flow rates in f_1, f_2 and f_3 could be conditioned and were gauged by flow meters “b_1”, “b_2” and “b_3” respectively. Moisture was removed again in f_3 via a diffusion dryer “d” (Model 3062, TSI). The processed air was finally supplied to the chamber through a high sidewall inlet “e_1” and exhausted through an outlet “e_2” aligned on the opposite chamber wall. Both the inlet and outlet were circular with a diameter of 0.016 m. Measurements were conducted at ventilation rates of 1.7, 10.3 and 18.8 h^{-1}, corresponding to inlet velocities of 0.17, 1 and 1.8 ms^{-1}, under isothermal conditions at an air temperature of 25°C and a relative humidity of 55%. All measurements were repeated three times and the average results were used in the analysis.

To check whether or not the vegetative bacterial cells/fungal spores appeared singly and without impurities, 0.01 ml suspension samples collected in the nebulizer were inspected microscopically. The whole suspension (50 ml) would be discarded if 2

out of 3 of its samples had 2% or more vegetative bacterial cells/fungal spores that failed the inspection. As substantial amounts of viable microorganisms will be lost after nebulization (e.g. due to the rapid loss of water), viability of the tested bacterial cells/fungal spores was also investigated after nebulization and dehumidification. Another 0.1 ml suspension collected at the inlet of the chamber was tested for the initial concentration of viable cells. Serial dilutions of the suspension were prepared using sterile Ringer's solution and then spread plated in triplicate on TSA and MEA. The plates were then incubated at 30 °C for 24 hours or 25 °C for 1 week for different types of bioaerosols. The concentration was expressed as CFU ml^{-1} after incubation. It was observed that 10-15% of the bacterial cells or fungal spores were lost after the process of nebulization and dehumidification. Sample bioaerosol particles were also scrutinized microscopically to verify the assumption that each colony formed on the agar plates arises from one cell. Experiments were started within one hour after the bioaerosol preparation for viability. For each test, bioaerosols were supplied into the chamber and air samples (each of 0.1 m^3) in the chamber were collected by Biostage Single-stage Viable Cascade Impactors before and after the experiments. Sample tests showed insignificant concentration trend during the sampling period of one hour ($p \geq 0.3$, t-test). The chamber plates were collected and colonies on each plate were inspected every day during the incubation period for colony counting. The chamber was sterilized before and after each measurement by 75% ethanol and a 30-min ultraviolet light irradiation.

Air samples collected for airborne bioaerosol counts were used to examine the chamber cleanliness.

4. Results and discussion

As depicted in Figure 3, deposition distributions on the chamber floor are expressed as the fractional bioaerosol counts $C_{e,i}$ measured on the TSA/MEA plates under tested conditions for all species using Equation (6) below, where $\phi_{e,ij}$ is the total bioaerosol counts at location ij, i=1,…,7 and j=1,…,4 are the array coordinates of the plates corresponding to the chamber fractional lengths x/l=0.069, 0.208, 0.346, 0.485, 0.623, 0.762, 0.9 and the chamber fractional widths y/w=0.125, 0.375, 0.625, 0.875 respectively.

$$C_{e,i} = \frac{\sum_{j} \phi_{e,ij}}{\sum_{i}\sum_{j} \phi_{e,ij}} \quad \ldots (6)$$

Experimentally, the total bioaerosol counts found on the chamber floor varied between 1,200 CFU to 28,000 CFU as shown in Table 2.

Computationally, a total of 11,500 bioaerosol particles (i.e. particle density = 0.2 CFU cm^{-3}) were injected at ventilation rates 1.7 h^{-1}, 10.3 h^{-1} and 18.8 h^{-1} and about

90%, 30% and 20% of the injected particles deposited on the chamber floor respectively. The particle tracking results are summarized in Table 2. Particles deposited in the defined longitudinal floor sections $\frac{1}{7}l, \frac{2}{7}l, \ldots, \frac{7}{7}l$ were counted as $\phi_{s,1}$, $\phi_{s,2}$, …, $\phi_{s,7}$ respectively. Using $C_{s,i} = \frac{\phi_{s,i}}{\sum_i \phi_{s,i}}$, the fractional depositions were calculated. The Reynolds numbers for the flow field in the chamber were 0.723 at 1.7 h^{-1}, 2.19 at 10.3 h^{-1} and 3.3 at 18.8 h^{-1}. Relative velocities of 100 randomly tracked equivalent particles and their corresponding ranges of Reynolds numbers are shown in Table 1. Particle tracking simulations were repeated 10 times for the same ventilation conditions. Averages of the fractional deposition are graphed in Figure 3. The computational predictions using the FLUENT default settings for K (=24 assumed for particles at a predicted Reynolds number Re<0.1 as presented in Table 1) were not promising: the fractional bias ε_1 was −7% (range −12% to 5%) and the normalized mean square error ε_2 was 15% (range 3% to 26%). Errors reported for bacteria were ε_1 = −9% (range −7% to −12%) and ε_2 = 18% (9% to 24%), whereas smaller errors ε_1 = −3% (range −8% to 5%) and ε_2 = 11% (3% to 26%) were found for fungi.

Figure 4 exhibits the results of absolute errors ε_1 and ε_2 from all measured flow conditions versus bioaerosol drag constants K and shows that K is a critical aerodynamic property for the bioaerosols. Except for the larger sized bioaerosols

Cladosporium and *Rhizopus*, the minimization of ε_1 and ε_2 gave $K<24$. The relevant range and average values of K are shown in Table 1. It was reported that out of the thirteen bioaerosol species tested, six had a range of K values below 1 while four had a range between 1 and 2. Moreover, *Serratia*, *Cladosporium* and *Rhizopus* had larger K values: 3.1, 14.9 and 22.8 respectively.

The drag coefficients C_D of the bioaerosols determined using the drag constants K are plotted against Reynolds numbers *Re* in Figure 5. It should be noted that the Reynolds numbers were in the range of 10^{-2} to 10^{-5}, except for those found to have higher values at the chamber inlet. The drag constant $K=24$ (in the *Re* range) for particles is shown in the figure for reference. Bacteria were found to be associated with drag constants ($K=0.2$ to 4.3) lower than $K=24$ ($p<0.0001$, *t*-test), whereas fungi generally had larger drag constants ($p<0.001$, *t*-test) in a wider range: the drag constant values for *Alternaria*, *Aspergillus* and *Penicillium* were significantly lower than $K=24$ ($p\leq0.01$, *t*-test), yet the ones for *Cladosporium* and *Rhizopus* were not ($p\geq0.2$, *t*-test). A low drag constant has significant influence on the drag force of the bioaerosol particles, and the choice of K has direct influence on the simulated deposition patterns.

Although the drag constant K showed no significant correlation with the aspect ratio l_b ($p=0.5$, *t*-test for no correlation), it was found to be correlated with the bioaerosol diameter d_b ($p<0.0001$, *t*-test for no correlation). Figure 6 is a plot of the drag constant K against the bioaerosol diameter d_b. $K=24$ would be a good approximate for

larger sized fungi such as *Rhizopus* (d_b=8.6 μm), but not for smaller sized fungi and bacteria. It should be noted that K=24 is assumed in the Reynolds number range in many bioaerosol simulations. With d_b up to 6.9 μm, K can be determined by,

$$K = \frac{d_b^2}{2};\ 0.69 \le d_b \le 6.9 \quad \text{... (7)}$$

$$K = 24;\ d_b > 6.9 \quad \text{… (8)}$$

In general, forces of gravity and inertia are proportional to the particle mass, which is proportional to d_b^3, whereas the particle surface area (and hence the electrostatic and van der Waals forces) is proportional to d_b^2. Therefore, as the particle size decreases, d_b^3 goes down much faster than d_b^2 so that the ratio of electrostatic and van der Waals to inertia and gravity forces becomes larger. The drag constant K was found to be approximately proportional to d_b^2 disregarding the particle shape and type. Figure 6 illustrates the good agreement between this finding and the experimental data for bioaerosols in the size range $0.69 \le d_b \le 6.9$.

Using Equation (7), fractional deposition patterns in the chamber were simulated and compared with the experimental ones and the results are exhibited in Figure 7 (calculated errors ε_1 and ε_2 are shown in Table 1 and graphed in Figure 8). The simulation results show that variations in deposition patterns are well described and the

simulation accuracy (expressed as lower absolute errors ε_1 and ε_2) is greatly improved (p<0.0001, t-test). The only two exceptions are: *Cladosporium* with no improvement and *Rhizopus* with insignificant improvement (p>0.1, t-test). It should be noted that as Equation (7) has a large variation in tested K values for *Cladosporium* (d_b=3.4 μm), its application in the d_b range between 3 μm and 6.9 μm may require further verification.

5. Conclusion

In practice, particle drag coefficient is usually calculated using empirical relations generalizing experimental data. This study demonstrated that using the FLUENT default Stokes' law settings to computationally predict drag coefficients for bioaerosols was not promising: the average fractional bias was 7% and the average normalized mean square error was 15%. Comparatively, errors reported for bacteria (−12% to 24%) were larger than those for fungi (−8% to 26%). These errors, however, can be minimized by a suitable choice of drag constant which can be determined by use of the bioaerosol diameter. This study also reported that bacteria were associated with average drag constants (0.25 to 3.1) much lower than 24, whereas fungi generally had larger drag constants in a wider range. Furthermore, the correlation between drag coefficient and Reynolds number for common indoor bioaerosols with diameters in between 0.69 μm and 8.6 μm was investigated. The outcome serves as a good reference

point for estimating the deposition distribution patterns of various common indoor bioaerosols.

Acknowledgment

The work described in this paper was partially supported by the grants from The Hong Kong Polytechnic University (Project account numbers G-U909 and G-YK22).

References

1. Yang Y, Sze-To GN and Chao CYH: Estimation of the Aerodynamic Sizes of Single Bacterium-Laden Expiratory Aerosols Using Stochastic Modeling with Experimental Validation. *Aerosol Sci Technol* 2012; 46: 1-12.
2. Tian L and Ahmadi G: Particle deposition in turbulent duct flows–comparision of different model predictions. *J Aerosol Sci* 2007; 38: 377-397.
3. Zhang Z and Chen Q: Experimental measurements and numerical simulations of particle transport and distribution in ventilated rooms. *Atmos Environ* 2006; 40: 3396-3408.
4. Zhao B and Wu J: Effect of particle spatial distribution on particle deposition in ventilation rooms. *J Hazard Mater* 2009; 170: 449-456.
5. Wang M, Lin CH and Chen Q: Determination of particle deposition in enclosed spaces by Detached Eddy Simulation with the Lagrangian method. *Atmos Environ* 2011; 45: 5376-5384.
6. Littman H, Morgan III MH, Paccione JD, Jovanovic SD: Modeling and measurement of the effective drag coefficient in decelerating and non-accelerating turbulent gas-solids dilute phase flow of large particles in a vertical transport pipe. *Powder Technol* 1993; 77: 267-83.
7. Petkov JT, Denkov ND, Danov KD, Velev OD, Aust R and Durst F: Measurement of the drag coefficient of spherical particles attached to fluid interfaces. *J Colloid Interface Sci* 1995; 172: 147-54.
8. Flórez-Acosta O, Tobón-Zapata G and Valencia-Velasquez J: Categorization of the main descriptors of different ampicillin crystal habits. *Braz J Pharm Sci*. 2010; 46: 679-685.
9. Almeida-Prieto S, Blanco-Méndez J and Otero-Espinar FJ: Microscopic image analysis techniques for the morphological characterization of pharmaceutical particles: Influence of the software, and the factor algorithms used in the shape factor estimation. *Eur J Pharm Biopharm* 2007; 67: 766-776.
10. Igathinathane C, Pordesimo LO, Columbus EP, Batchelor WD and Methuku SR: Shape identification and particles size distribution from basic shape parameters using ImageJ. *Comput. Electron Agric* 2008; 63: 168-182.
11. Blott SJ and Pye K: Particle shape: a review and new methods of characterization and classification. *Sedimentology* 2008; 55: 31-63.
12. Wong LT, Chan WY, Mui KW and Lai ACK: An Experimental and Numerical Study on Deposition of Bioaerosols in a Scaled Chamber. *Aerosol Sci Technol* 2010; 44: 117-128.
13. ASTM: Standard Guide for Statistical Evaluation of Atmospheric Dispersion Model Performance D6589-05(2010)e1. West Conshohocken, PA.: *ASTM* 2010.
14. Roache PJ: Verification of Codes and Calculations. *AIAA Journal*. 1998; 36: 696-702.

15. Hussein T, Hruska A, Dohanyosova P, et al: Deposition rates on smooth surfaces and coagulation of aerosol particles inside a test chamber. *Atmos Environ* 2009; 43: 905-14.
16. Rim D, Green M, Wallace L, Persily A and Choi JI: Evolution of Ultrafine Particle Size Distributions Following Indoor Episodic Releases: Relative Importance of Coagulation, Deposition and Ventilation. *Aerosol Sci Technol* 2012; 46: 494-503.
17. Lai ACK, Wong LT, Mui KW, Chan WY and Yu HC: An experimental study of bioaerosol (1-10μm) deposition in a ventilated chamber. *Build Environ* 2012; 56: 118-126.
18. Pastuszka JS, Kyaw Tha Paw U, Lis DO, Wlazlo A and Ulfig K: Bacterial and fungal aerosol in indoor environment in Upper Silesia, Poland. *Atmos Environ* 2000; 34: 3833-3842.
19. Su HJ, Chen HL, Huang CF, Lin CY, Li FC and Milton DK: Airborne fungi and endotoxin concentrations in different areas within textile plants in Taiwan: a 3-year study. *Environ Res* 2002; 89: 58-65.
20. Shelton BG, Kirkland KH, Flanders WD and Morris GK: Profiles of Airborne Fungi in Buildings and Outdoor Environments in the United States. *Appl Environ Microbiol* 2002; 68: 1743-1753.
21. Kemp PC, Neumeister-Kemp HG, Esposito B, Lysek G and Murray F: Changes in airborne fungi from the outdoors to indoor air; large HVAC systems in nonproblem buildings in two different climates. *Am Ind Hyg Assoc J* 2003; 64: 269-275.
22. Bouillard L, Michel O, Dramaix M and Devleeschouwer M: Bacterial contamination of indoor air, surfaces, and settled dust, and related dust endotoxin concentrations in healthy office buildings. *Ann Agric Environ and Med* 2005; 12: 187-192.
23. Seino K, Takano T, Nakamura K and Watanabe M: An evidential example of airborne bacteria in a crowded, underground public concourse in Tokyo. *Atmos Environ* 2005; 39: 337-341.
24. Wu PC, Li YY, Chiang CM, et al: Changing microbial concentrations are associated with ventilation performance in Taiwan's air-conditioned office buildings. *Indoor air*. 2005; 15: 19-26.
25. Kim KY and Kim CN: Airborne microbiological characteristics in public buildings of Korea. *Build Environ* 2007; 42: 2188-2196.
26. Aydogdu H, Asan A and Tatman Otkun M: Indoor and outdoor airborne bacteria in child day-care centers in Edirne City (Turkey), seasonal distribution and influence of meteorological factors. *Environ Monit Assess* 2010; 164: 53-66.
27. Chan PL, Yu PHF, Cheng YW, Chan CY and Wong PK: Comprehensive characterization of indoor airborne bacterial profile. *J Environ Sci* 2009; 21: 1148-1152.

28. Chan WY: A study of bio-risk assessment, control and evaluation (BRACE) for indoor environment. *Building Services Engineering*. Hong Kong: The Hong Kong Polytechnic University, 2012.
29. Wagner J and Macher J: Automated Spore Measurements Using Microscope, Image Analysis, and Peak Recognition of Near-Monodisperse Aerosols. *Aerosol Sci Technol* 2003; 46: 862-873.
30. Ferreira T and Rasband W: ImageJ User Guide / Fiji 1.46. 2012.

Table 1. Common indoor airborne bacteria and fungi

Genera/Species	Relative abundance	ATCC no.	SEM samples	Bioaerosol diameter d_b (μm)[a]	Aspect ratio l_b	Reynolds number Re ($\times 10^{-5}$)	Relative velocity ($\times 10^{-6}$ ms^{-1})	Bioaerosol drag constant K	K=24		$K=d_b^2/2$	
									ε_1	ε_2	ε_1	ε_2
(a) Bacteria												
Aeromonas hydrophila	<1%	-	35	1.8±0.05	2.9	84-2410	0.005-0.20	1.60 (1.5-1.7)	–0.084	0.200	0.001	0.119
Bacillus atrophaeus	1-19%	9372	17	1.1±0.04	2.2	38-1290	0.006-0.18	0.55 (0.4-1.0)	–0.103	0.192	–0.001	0.040
Campylobacter jejuni	<1%	-	31	2±0.11	3.1	86-2620	0.005-0.18	2.15 (1.2-3.1)	–0.080	0.146	–0.003	0.069
Escherichia coli	<1%	10536	21	1±0.07	1.7	55-1270	0.005-0.17	0.60 (0.5-0.7)	–0.093	0.243	0.001	0.106
Micrococcus luteus	9-76%	4698	55	0.7±0.02	1.1	32-867	0.006-0.19	0.25 (0.2-0.3)	–0.115	0.228	–0.006	0.043
Salmonella typhimurium	<1%	14028	18	1.5±0.06	3.2	57-1970	0.005-0.17	1.85 (1.2-2.5)	–0.098	0.152	–0.024	0.035
Serratia marcescens	<1%	6911	41	2.6±0.07	6.9	2-3160	0.005-0.17	3.10 (1.9-4.3)	–0.067	0.086	0.001	0.050
Staphylococcus aureus	5-100%	-	28	0.69±0.02	1.0	31-867	0.005-0.19	0.25 (0.2-0.3)	–0.111	0.189	–0.004	0.042
(b) Fungi												
Alternaria alternata	0-4%	6663	4	3±0.78	1.4	17-3880	0.005-0.18	3.00 (3.0-3.0)	–0.075	0.259	–0.016	0.048
Aspergillus niger	9-20%	-	25	3±0.05	1.2	43-5370	0.005-0.18	4.20 (3.3-5.1)	–0.063	0.117	–0.002	0.052
Cladosporium cladosporioides	17-22%	16021	56	3.4±0.09	2.1	12-3950	0.005-0.18	14.9 (1.4-28.3)	0.050	0.054	0.068	0.071
Penicillium citrinum	8-34%	6849	23	2.5±0.04	1.1	96-2860	0.006-0.19	7.80 (7.0-8.6)	–0.032	0.029	0.003	0.011
Rhizopus	0-2%	-	39	8.6±0.25	1.0	55-10400	0.008-0.20	22.8 (19.5-26.1)	–0.012	0.113	–0.010	0.099

[a] Standard errors shown

Table 2. Particle tracking results

Species	Simulated particle counts in the experimental chamber (total injected count = 11500)				Total bioaerosol counts on the experimental chamber floor
	Floor	Outlet	Wall	Suspended in air	
Ventilation Rate = 1.7 h^{-1}					
A. hydrophila	10145	1011	344	0	3598
B. atrophaeus	10170	986	344	0	28276
C. jejuni	10222	930	348	0	17431
E. coli	10222	930	348	0	7883
M. luteus	10158	1008	334	0	3067
S. typhimurium	10159	975	366	0	15164
S. marcescens	10158	987	355	0	16349
S. aureus	10111	1015	374	0	5733
A. alternata	10159	975	366	0	4709
A. niger	10159	975	366	0	3375
C. cladosporioides	10148	983	369	0	4251
P. citrinum	10191	976	333	0	5973
Rhizopus sp.	10107	1024	369	0	4865
Ventilation Rate = 10.3 h^{-1}					
A. hydrophila	3243	6879	1376	2	13403
B. atrophaeus	3257	6802	1439	2	8697
C. jejuni	3320	6819	1355	6	18761
E. coli	3320	6819	1355	6	8047
M. luteus	3283	6872	1341	4	6246
S. typhimurium	3283	6824	1389	4	16544
S. marcescens	3201	6958	1337	4	4889
S. aureus	3232	6919	1343	6	9318
A. alternata	3283	6824	1389	4	3777
A. niger	3283	6824	1389	4	1269
C. cladosporioides	3246	6873	1375	6	5208
P. citrinum	3289	6838	1366	7	5547
Rhizopus sp.	3270	6885	1341	4	3035
Ventilation Rate = 18.8 h^{-1}					
A. hydrophila	2453	7716	1329	2	5509
B. atrophaeus	2391	7731	1370	8	3318
C. jejuni	2430	7740	1323	7	2972
E. coli	2430	7740	1323	7	14611
M. luteus	2540	7669	1284	7	1644
S. typhimurium	2412	7792	1292	4	10481
S. marcescens	2454	7738	1303	5	13507
S. aureus	2417	7782	1296	5	5437
A. alternata	2412	7792	1292	4	4403
A. niger	2412	7792	1292	4	1219
C. cladosporioides	2475	7726	1292	7	1230
P. citrinum	2403	7764	1328	5	2995
Rhizopus sp.	2459	7706	1323	12	3556

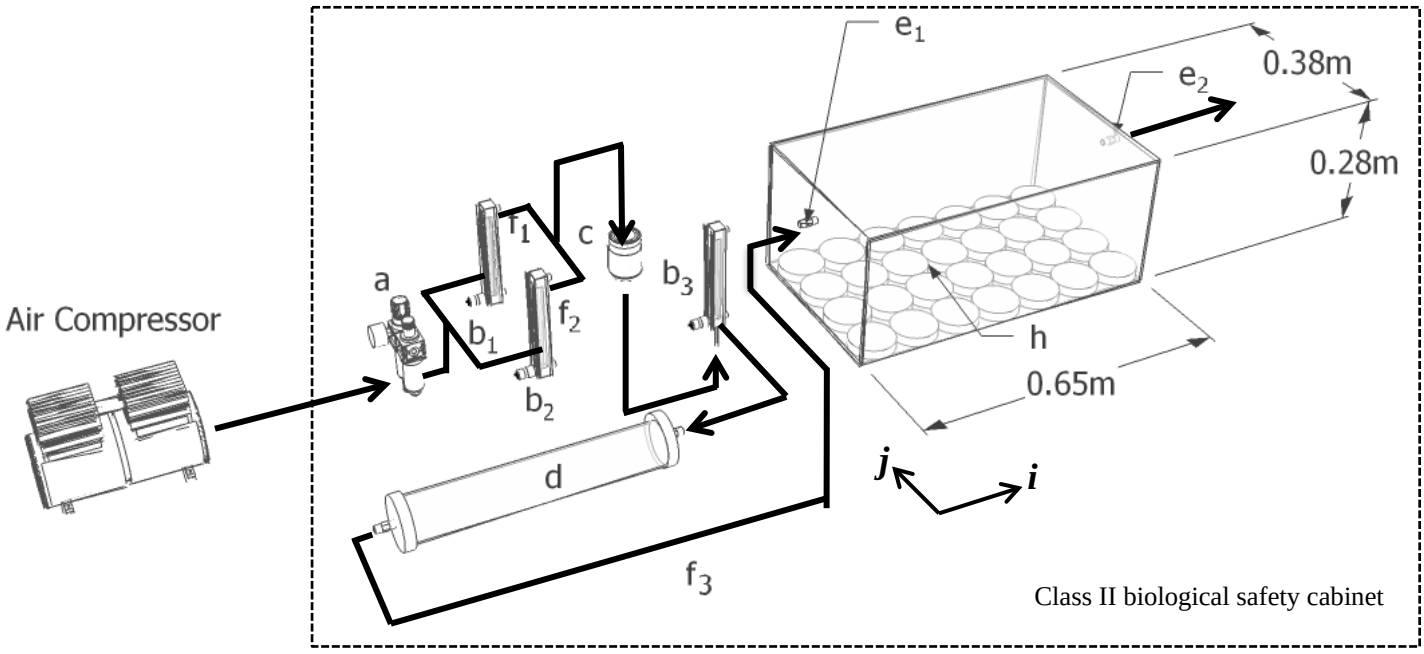

a	filtration system	d	diffusion dryer
b_1,b_2,b_3	flow meters	e_1	inlet
c	6-jet collision nebulizer or aerosolization chamber for bioaerosols with diameter > 3μm*	e_2	outlet
		f_1,f_2,f_3	airflow paths
		h	agar plate array

* Details of aerosolization chamber "c" for bioaerosols with diameter > 3μm

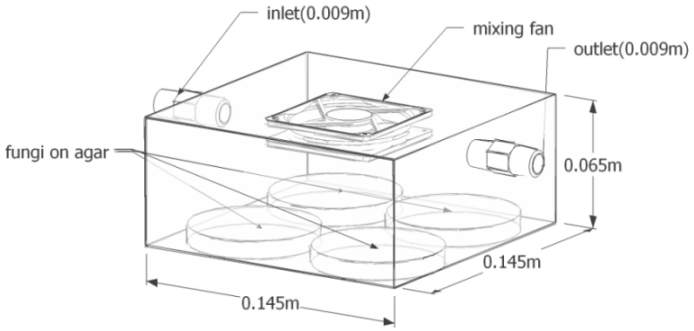

Figure 1. Chamber setup

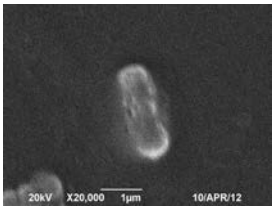

Aeromonas hydrophila

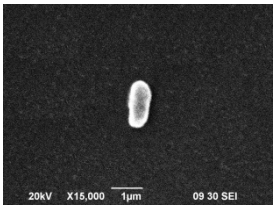

Bacillus atrophaeus (ATCC 9372)

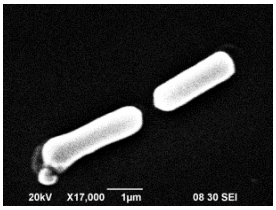

Campylobacter jejuni

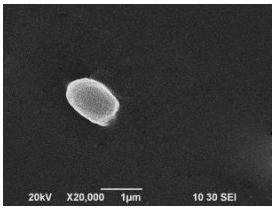

Escherichia coli (ATCC 10536)

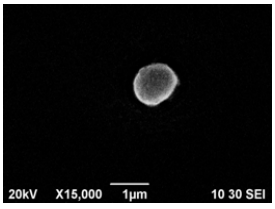

Micrococcus luteus (ATCC 4698)

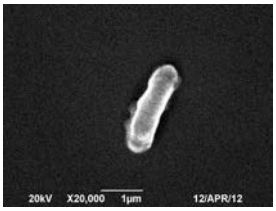

Salmonella typhimurium (ATCC 14028)

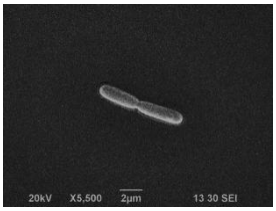

Serratia marcescens (ATCC 6911)

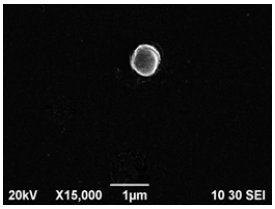

Staphylococcus aureus (ATCC 6538)

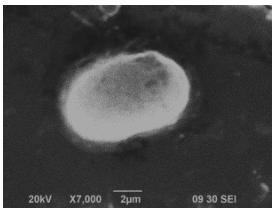

Alternaria alternata (ATCC 6663)

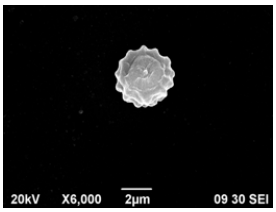

Aspergillus niger

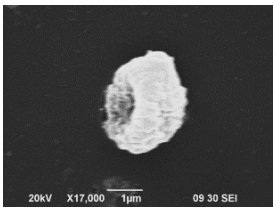

Cladosporium cladosporioides (ATCC 16021)

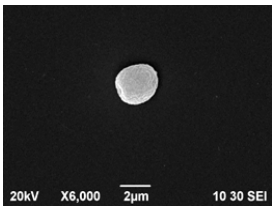

Penicillium citrinum (ATCC 6849)

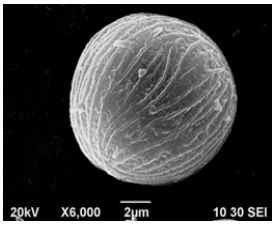

Rhizopus sp.

Figure 2. Reference indoor airborne bacteria and fungi

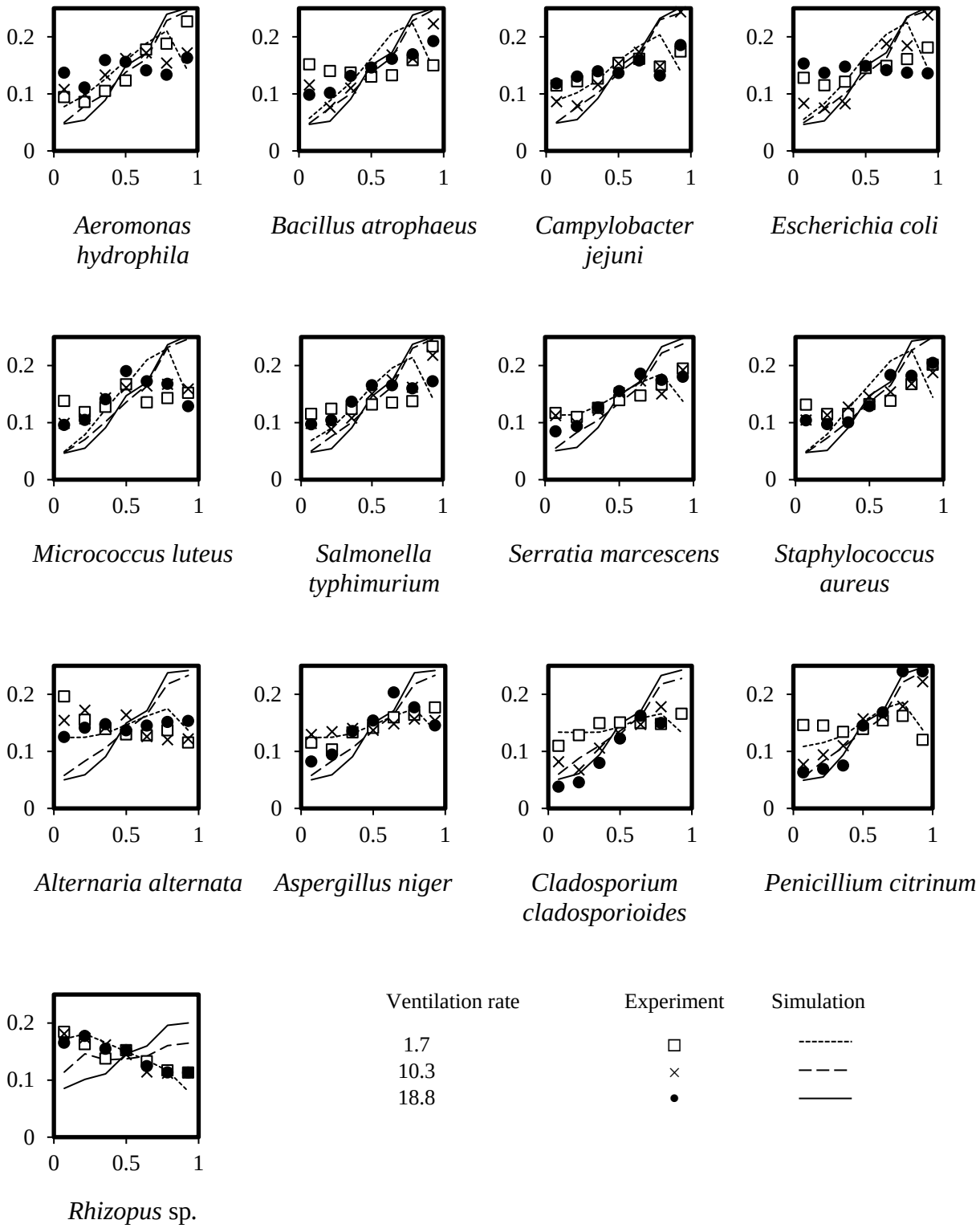

x-axis: Fractional distance from air inlet
y-axis: Fractional bioaerosol counts

Figure 3. Fractional bioaerosol counts on the chamber floor with *K* for particle simulations

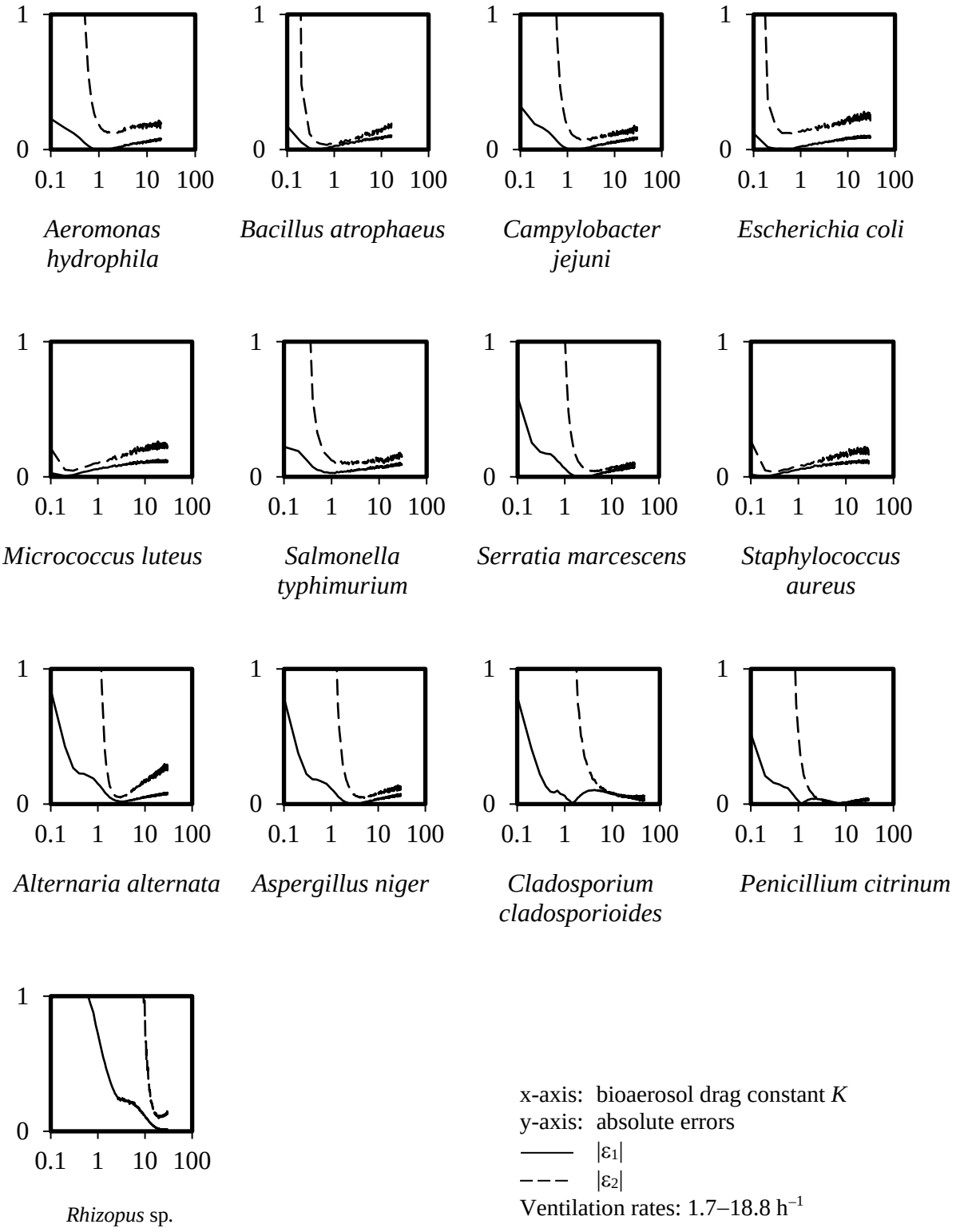

Figure 4. Bioaerosol drag constants and absolute errors

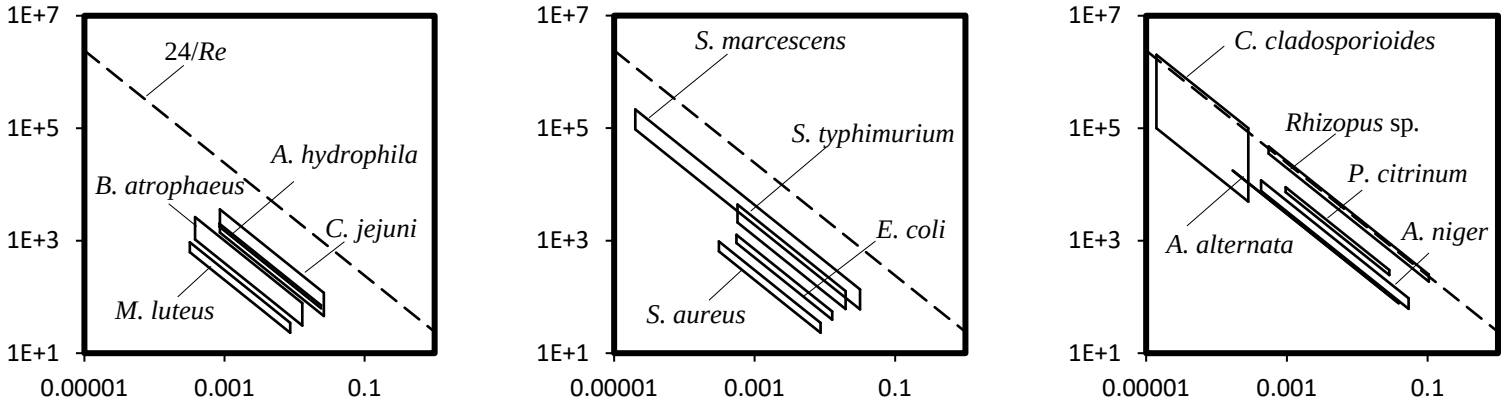

x-axis: (Relative) Reynolds number *Re*
y-axis: Bioaerosol drag coefficient

Figure 5. Bioaerosol drag constant against Reynolds number of equivalent particles

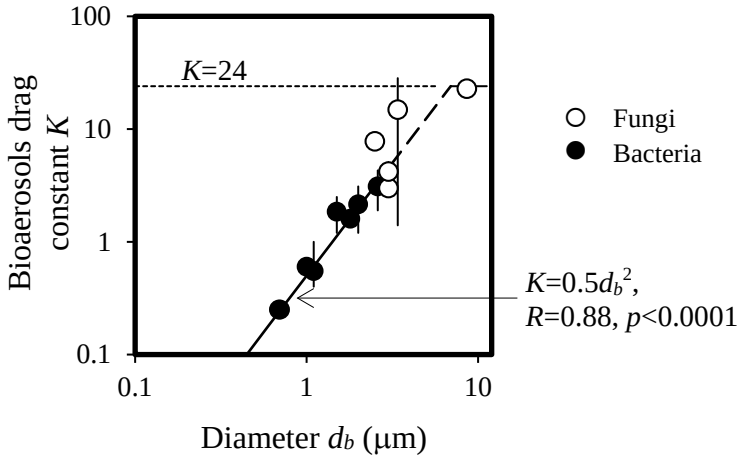

Figure 6. Bioaerosol drag constant *K* against bioaerosol diameter d_b

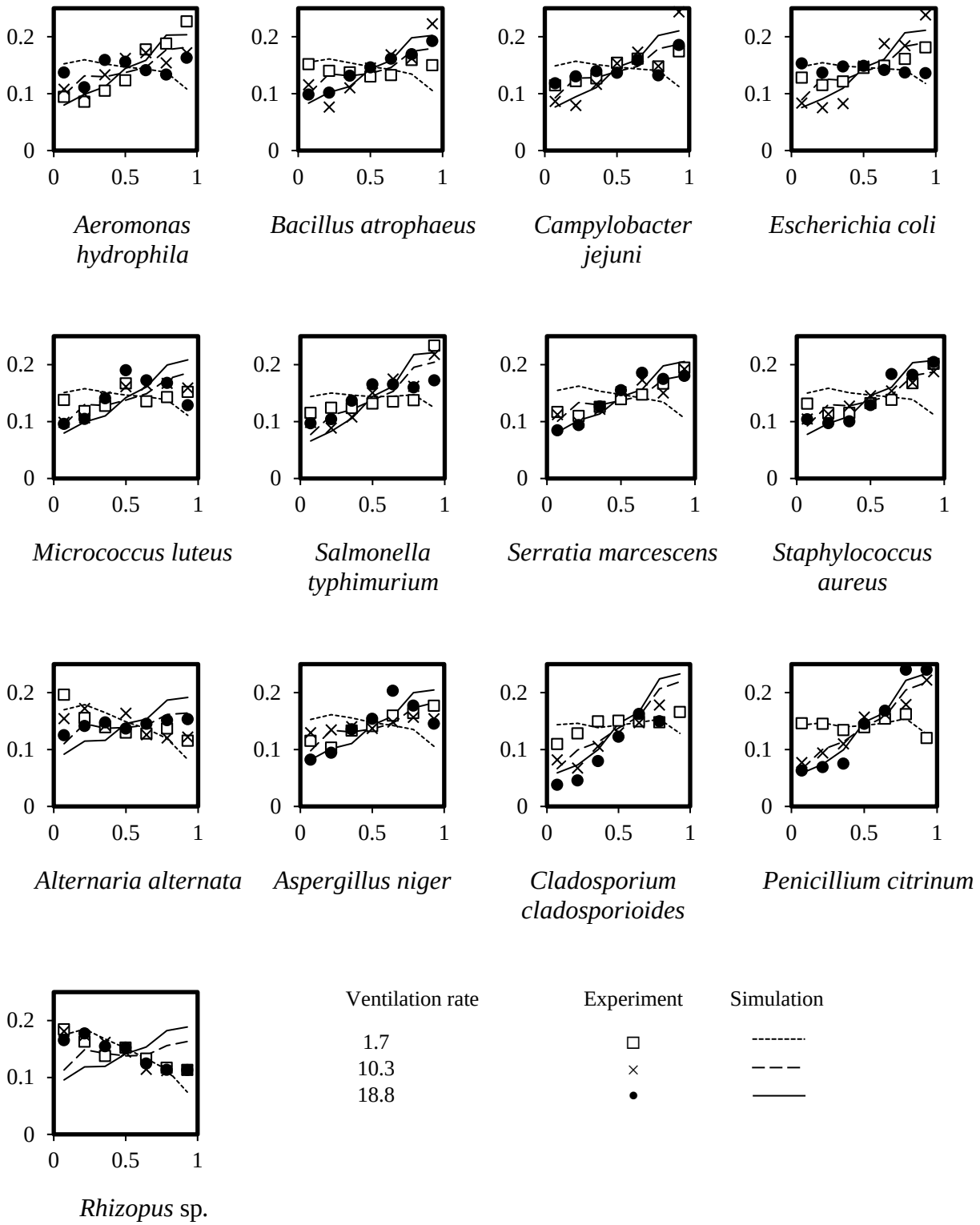

x-axis: Fractional distance from air inlet
y-axis: Fractional bioaerosol counts

Figure 7. Fractional bioaerosol counts on the chamber floor with bioaerosol drag constant *K*

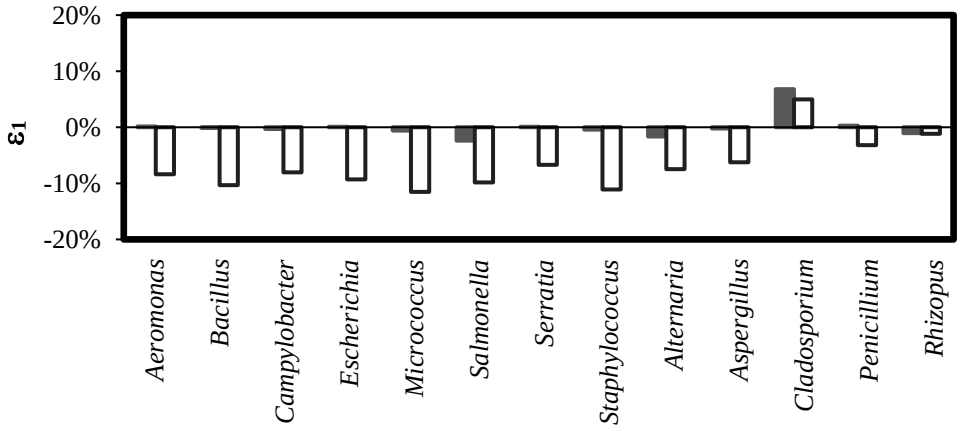

(a) ε_1

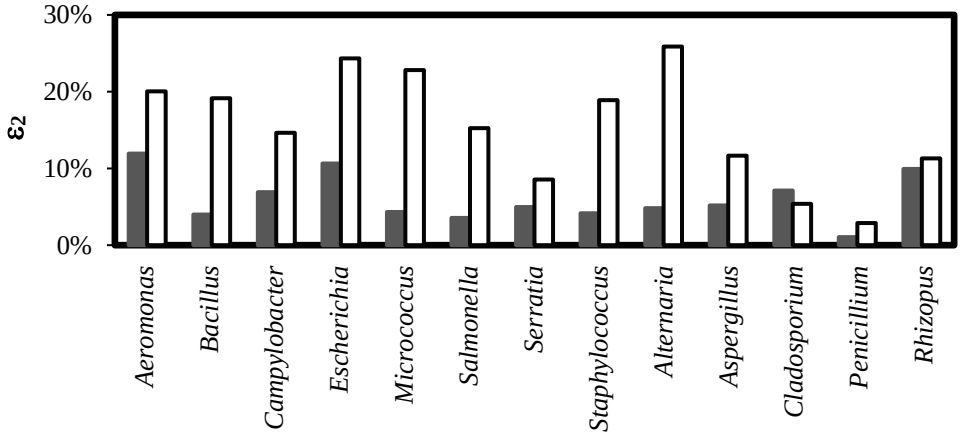

(b) ε_2

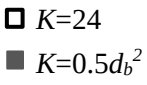

Figure 8. Errors between simulated and measured bioaerosol deposition patterns